Acta Crystallographica Section B
Structural Science
ISSN 0108-7681

Synchrotron powder diffraction characterization of the zeolite-based (*p*-*N*,*N*-dimethylnitroaniline–mordenite) guest–host phase

Florence Porcher,[a] Elena Borissenko,[a] Mohamed Souhassou,[a] Masaki Takata,[b,c,d] Kenichi Kato,[b,c,e] Juan Rodriguez-Carvajal[f] and Claude Lecomte[a]*

[a]LCM3B, UMR 7036 CNRS, Nancy Université, Université Henri Poincaré, BP 239, 54506 Vandoeuvre-lès-Nancy, France, [b]RIKEN SPring-8 Center, 1-1-1 Kouto, Sayo-cho, Sayo-gun, Hyogo 679-5148, Japan, [c]Japan Synchrotron Radiation Research Institute, 1-1-1 Kouto, Sayo-cho, Sayo-gun, Hyogo 679-5198, Japan, [d]Department of Advanced Materials Science, The University of Tokyo, 5-1-5 Kashiwanoha, Kashiwa, Chiba 277-8561, Japan, [e]Japan Science and Technology Agency, 4-1-8 Honmachi, Kawaguchi, Saitama 332-0012, Japan, and [f]Institut Laue–Langevin, 6 rue Jules Horowitz, BP 156 38042 Grenoble CEDEX 9, France

Correspondence e-mail: claude.lecomte@lcm3b.uhp-nancy.fr

Received 20 December 2007
Accepted 5 August 2008

The crystal structure of a new phase consisting of the inclusion of the hyperpolarizable molecule *p*-*N*,*N*-dimethylnitroaniline (*dim*ethyl-*p*ara-*n*itro*a*niline or dmpNA) in the large-pore zeolite mordenite (MOR) has been determined from high-resolution synchrotron powder diffraction at 300 and 90 K. The unit-cell parameters and space group at 300 K are similar to those of as-synthesized mordenite. The crystallographic study indicates that the MOR straight channels are almost fully loaded with molecules that are disordered over eight symmetry-related sites. As expected, the molecules are located in the large 12-membered ring channel, at the intersection with the secondary eight-membered channel with which they might form hydrogen bonds. The elongation axes (and then the dipole moments) of the molecules are slightly tilted (28.57°) from [001]. The configuration found suggests an interaction of dmpNA with framework O atoms through its methyl groups.

1. Introduction

Various matrices (amorphous silica gels and glasses, polymers and micro-/mesoporous) have been studied in the past decade in order to disperse and stabilize functional organic molecules and to produce performing materials for non-linear optics: second harmonic generation (SHG), parametric amplification, optoelectronics (signal amplification and routing), compact and accordable microlasers, and optical memories (Schulz-Ekloff *et al.*, 2002; Laeri *et al.*, 2003).

For the non-linear optics (NLO) materials, the performances are driven by the chromophore loading, the magnitude of the product of the dipole moment and first-order hyperpolarizability, and the coupling between dipole moments and the electric field responsible for molecular alignment. The more commonly used matrices are oriented films of organic materials based on polymers where the dipolar molecules are scattered throughout the layer; a limited ordering is generally achieved by electric field poling. These materials are easy to elaborate and cheap, but suffer from thermal instability and, from a more fundamental point of view, are difficult to model at the molecular level because of their intrinsic disordered nature.

The use of molecular sieves (zeolite analogues/mesoporous materials) possessing cages and channels of uniform size enables the incorporation of guest molecules in well defined positions. Contrary to the usual applications of zeolites as selective sorbants or catalysts where the complex has only a transient character and in which adsorbed molecules are highly mobile over interaction sites, in (chromophore–zeolite) complexes one has to reach a permanent and controlled arrangement of molecules. In both cases detailed under-

© 2008 International Union of Crystallography
Printed in Singapore – all rights reserved

standing of the guest–host interactions (Schulz-Ekloff *et al.*, 2002; Laeri *et al.*, 2003) is a primary step to construct functional materials tailored at a molecular level since the properties of the hybrid compound depend on the guest–host interactions (such as hydrogen bonding, ion pairs, hydrophobic interaction). Zeolite-based guest–host systems have been probed locally by NMR (Shantz & Lobo, 1999; Fyfe & Brouwer, 2000; Komori & Hayashi, 2003*a*,*b*), UV–vis (Hoffmann, Marlow, Caro & Dähne, 1996; Calzaferri *et al.*, 2000) and Raman–IR spectrometries (Dutta, 1995), resulting in an indirect insight into the chromophore–matrix interactions. Only a few diffraction experiments have been performed on the mordenite-based guest–host phase in order to probe the interactions at the molecular level in crystalline microporous materials, despite it being the most accurate method (van Koningsveld & Koegler, 1997; Reck *et al.*, 1996; Mentzen & Lefebvre, 1998; Ghermani *et al.*, 1996; Kuntzinger *et al.*, 1998; Aubert *et al.*, 2002, 2003, 2004).

Mordenite (MOR) zeolite was initially chosen because it offers a one-dimensional channel system (Fig. 1) wider than that of previously studied MFI or AFI frameworks (Caro *et al.*, 1992; Marlow *et al.*, 1993; Caro *et al.*, 1994; Marlow *et al.*, 1994; Hoffmann, Marlow & Caro, 1996); therefore, it is expected to accommodate larger and more interesting guest molecules. In its low-alumina form, it is also highly transparent in the near-UV–vis ($\lambda > 300$ nm) optical range.

As an organic guest, the model push–pull molecule *p*-*N*,*N*-dimethylnitroaniline (dmpNA), derived from paranitroaniline (pNA), was chosen (Komori & Hayashi, 2003*a*; Hoffmann, Marlow, Caro & Dähne, 1996; van Koningsveld & Koegler, 1997; Reck *et al.*, 1996). Its dimensions, compared with the channels of MOR, are shown in Fig. 2. Its length is such that one can foresee an alignment of the molecules along the channels. As the width of dmpNA is almost half the pore size, one can also expect to achieve high loading, favourable for optical properties and X-ray diffraction, together with a slight disorder.

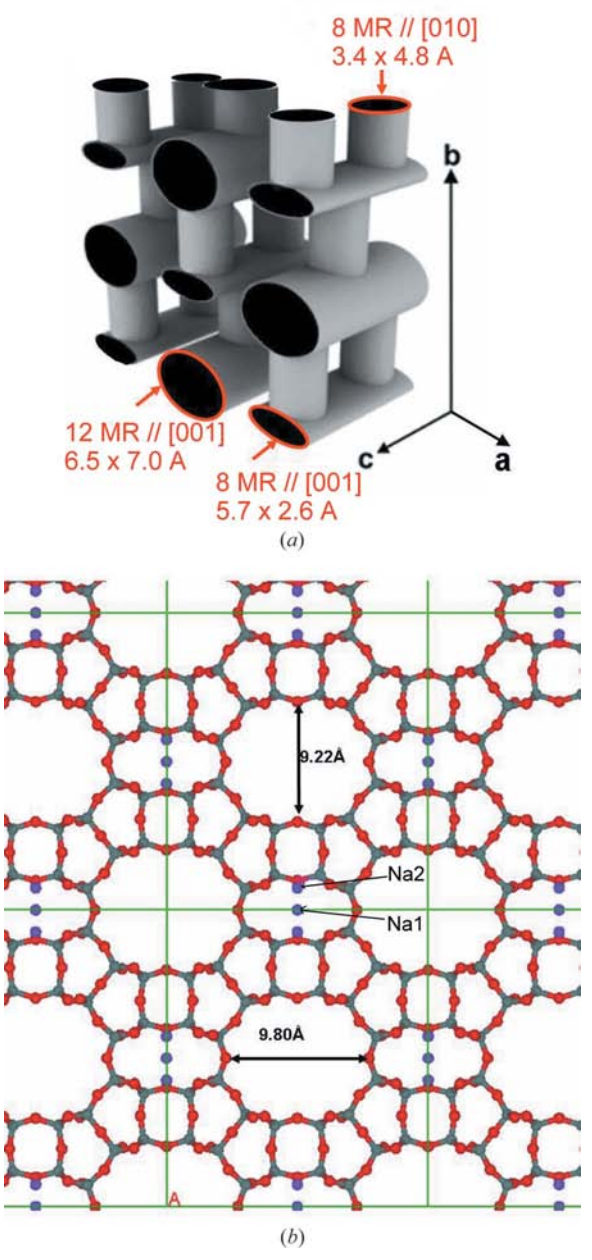

Figure 1
(*a*) Topology of MOR structural type; (*b*) cation sites and dimensions of channel apertures in mordenite calculated from nuclei positions without taking into account van der Waals radii.

2. Experimental

2.1. Sample preparation and optical characterization

Mordenite crystalline powder was produced according to the protocol proposed by Sano *et al.* (2001), with the addition of 1-butanol (BuOH) in order to enhance the crystallinity. We used double distilled water and commercially available reactant sources: silica (flocculent SiO_2 from Merck, purity 99–100.5% and Cabosil M-5 from Riedel-de Haën), sodium hydroxide (NaOH pellets, Carlo Erba, purity > 99%), aluminium nitrate [$Al(NO_3)\cdot x9H_2O$ Riedel-de-Haën, purity < 98%], butanol-1 (Fluka, purity < 98%), *p*-*N*,*N*-dimethylnitroaniline (Lancaster, purity < 98%).

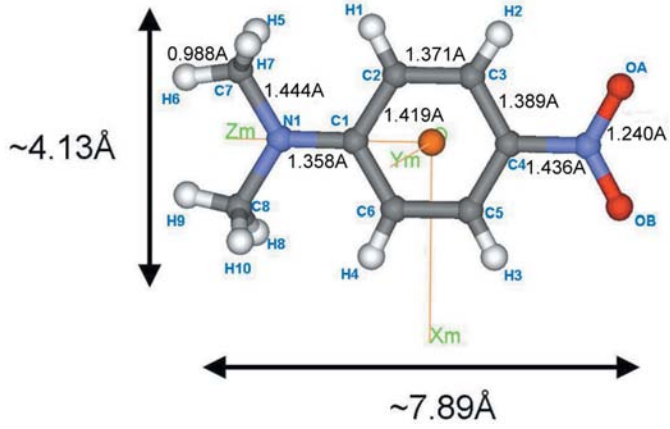

Figure 2
Schematic representation of the dmpNA molecule and its local frame axes.

Table 1
Agreement factors at the various refinement steps.

First value: agreement factor calculated over all 2θ range ($25 < 2\theta < 74.5°$); second value: agreement factor for $20 < 2\theta < 74.5°$ range.

Refinement data ($2.5 < 2\theta < 74.5°$)/($20 < 2\theta < 74.5°$)	R_p	R_{wp}	χ^2	R_{Bragg}	R_F
90 K dataset					
Pattern matching (LeBail fit)					
(1) Pattern matching	0.0142/–	0.0218/–			
Refinement of mordenite host					
(2) (Si, O) framework	0.426/0.169	0.770/0.172	2310/36.9	0.402/0.121	0.0946/0.0833
(3) (Si, O) framework + Na1 + Na2 Free Na1 and Na2 occupancies	0.399/0.130	0.885/0.128	3050/20.3	0.376/0.0864	0.0744/0.0658
Refinement of mordenite + dmpNA (simulated annealing + rigid body)					
(3bis) (Si, O) framework + Na1 + Na2 + dmpNA from simulated annealing Free Na1 and Na2 occupancies	0.126/0.133	0.147/0.132	83.6/21.4	0.0947/0.0892	0.0682/0.0670
4.1 Constrained Na1 and Na2 occupancies	0.0977/0.126	0.0924/0.126	33.7/19.9	0.0469/0.0677	0.0425/0.0439
4.2 Free Na1 and Na2 occupancies	0.0893/0.120	0.0846/0.120	28.3/18.2	0.0395/0.0623	0.0373/0.0390
Inversion of methyl-nitro moieties of dmpNA					
Constrained Na1 and Na2 occupancies	0.0987/0.127	0.0947/0.126	35.3/20.1	0.0488/0.0692	0.0450/0.0463
Free Na1 and Na2 occupancies	0.0910/0.123	0.0870/0.123	29.9/18.9	0.0391/0.0651	0.0407/0.0425
Refinement of mordenite + dmpNA (electron density tube)					
(5) Best disordered model (tube $1.00 < r < 2.50$ Å)	0.143/0.149	0.162/0.147	103.0/27.2	0.0784/0.0912	0.0578/0.0578
300 K dataset					
Full refinement, same hypothesis as 4.2 at 90 K	0.0868/0.113	0.0862/0.116	30.6/16.8	0.0411/0.0596	0.0375/0.0387

The synthesis gel, of molar composition $3.33H_2O$ + $0.06NaOH$ + $0.0024Al(NO_3)_2$ + $0.083SiO_2$, was first homogenized over 2 h at 338 K, then again 15 min after the final addition of 0.124BuOH. Finally, it was transferred into a Teflon-lined stainless steel autoclave, which was subsequently kept for 3 weeks at 423 K. The precipitated crystals ($\sim 40 \times 30 \times 20\ \mu m^3$, pure phase but aggregated) were filtered off, washed thoroughly with deionized water and dried. From microprobe and thermogravimetric analyses, the composition of the powder was estimated to be $Na_{0.15\ (3)}Al_{0.14\ (4)}Si_{1.00\ (1)}O_{2.28\ (1)}\cdot 0.455H_2O$.

After normalization to 48 *T* atoms (*T* = Si, Al in tetrahedral coordination) per unit cell, this gives an IZA (International Zeolite Association) IUPAC notation of $|Na_{6.3}(H_2O)_{19.1}|$-$[Al_{5.88}Si_{42.12}O_{96}]$·MOR {[001](12-ring)} (*Cmcm*).

Before vapour phase incorporation of dmpNA, the $\sim$ 12% weight H_2O was eliminated by heating the powder up to 673 K for 3 d. Loading with dmpNA was performed immediately afterwards, in order to prevent rehydratation, by enclosing under vacuum zeolite and dmpNA powders in a Pyrex tube, and heating at $\sim$ 403 K. After 5 d, (dmpNA-MOR) crystals had turned from white to yellow and no further change of colour was noticed. The UV–vis reflectance spectrum of the (dmpNA-MOR) powder was measured on a Varian Cary 4000 spectrometer equipped with an internal integration sphere, and converted in absorption scale *via* the Kubelka–Munk algorithm (*Cary WinUV* software; http://www.varianinc.com). It shows the characteristic broad band of $n - \pi^*/\pi - \pi^*$ transitions of dmpNA (Fig. 3). The two transitions are not resolved, contrary to crystalline dmpNA, and are blue shifted. The charge-transfer absorption band of MOR, at $\lambda \simeq$ 300 nm, does not overlap with the dipolar transitions, and does not preclude the *a priori* SHG properties of this material. Exhaustive optical characterizations, necessary to confirm the SHG expected in (dmpNA-MOR) and already observed in other channel-type zeolites (Reck *et al.*, 1996; Marlow *et al.*, 1993, 1994), are planned.

2.2. X-ray diffraction experiment

Before the diffraction experiment (dmpNA-MOR) crystals were ground with a pestle and mortar in a glovebox in a purified Ar gas environment. The powder was then introduced in a Lindemann glass capillary (Hilgenberg Gmbh, inner diameter 0.3 mm, wall thickness 0.01 mm) that was sealed *in vacuo*.

Synchrotron X-ray diffraction experiments [λ = 1.00171 (1) Å, calibrated with CeO_2 NIST 674a] were carried out on beamline BL02B2 (SPring-8, Hyogo Prefecture, Japan) at 300 and 90 K using the N_2 gas-flow system. The diffraction

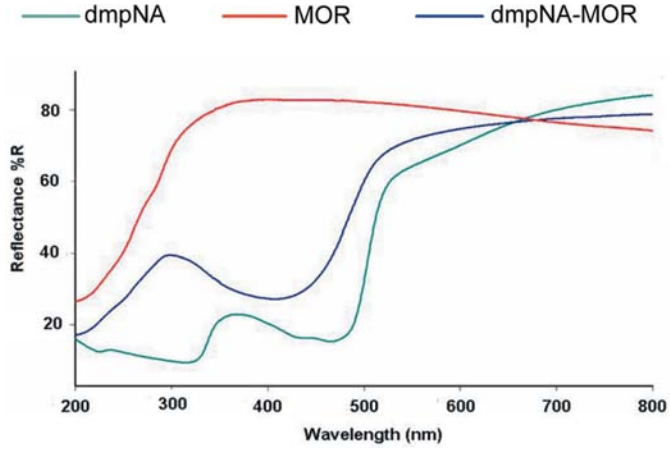

Figure 3
UV–vis spectra of dmpNA, as-synthesized mordenite and (dmpNA-MOR) powders (diffuse scattering, reflectance mode).

patterns were recorded in transmission geometry in the range $2.0 < 2\theta < 75.1^\circ$ [$(\sin\theta/\lambda)_{max}$ = 0.605 Å^{-1}], using an image-plate detector (Takata *et al.*, 2002; Matsuda *et al.*, 2005; Kubota *et al.*, 2006). Structure refinements were performed with the *FULLPROF* suite of programs (Rodriguez-Carvajal, 1993).

3. Results

3.1. Structure determination and refinement strategy (90 K experiment)

The 90 K diffraction pattern was indexed with the program *DicVol* (Boultif & Louër, 1991) in an orthorhombic cell [a = 20.402 (1), b = 18.038 (1), c = 7.4976 (4) Å] using 84 lines, with figures of merit $M(20)$ = 117.6, $F(20)$ = 388.4 (de Wolff, 1968; Smith & Snyder, 1979). No violation of the C-centring systematic absences was observed and the space group *Pbcn* (Schlenker *et al.*, 1979) was discarded. The pattern matching (LeBail fit; LeBail *et al.*, 1988), restricted to the $2.5 < 2\theta < 74.5^\circ$ range covering the effective measurement, was satisfactory with the space group *Cmcm* which is usually accepted for mordenite (R_p = 0.0142, R_{wp} = 0.0218, Table 1); all diffraction peaks, except one very weak peak at $2\theta = 5.2^\circ$ (assigned to an impurity), were calculated. Profiles were modelled using a pseudo-Voigt peak-shape function (Thompson *et al.*, 1987) including correction for axial divergence asymmetry (Finger *et al.*, 1994) for low-angle peaks ($2\theta < 15^\circ$).

The starting structural model was derived from a previous structure of a dehydrated mordenite of similar composition solved in LCM^{3}B (Nancy, to be published). All tetrahedral sites were modelled with Si atoms, neglecting the ∼12.5% amount of Al atoms. Displacement parameters were constrained for chemically equivalent atoms. The model first included only the framework atoms, as Na^+ cations were suspected to move upon the absorption of guest molecules (Komori & Hayashi, 2003*b*).

Any attempt to refine atomic positions and displacement parameters over the complete 2θ range failed because of the poor fit of the intense low-resolution peaks ($2\theta < 20^\circ$). Such behaviour is expected if a disordered fragment is lacking in the model. As a consequence, refinements were first performed in the $20 < 2\theta < 74.5^\circ$ range, where only the well ordered part of the structure contribute significantly. With that restriction, refinements converged readily. In fact, the agreement factors for the whole pattern ($2.5 < 2\theta < 74.5^\circ$, Table 1) were also calculated without refinement for the sake of comparison with further steps. At this refinement stage, successive difference-Fourier syntheses allowed the localization of Na^+ cations; unexpectedly, these latter cations occupy the same two sites inside the elliptic 8MR channels as those found in a previous study of dehydrated MOR. As shown on Table 1, the introduction of the Na^+ cations improved the fit significantly, but not for the low-order angular range (Figs. 4*a* and *b*). The disagreement of the fit shows the major contribution of the guest molecule to the low-angle reflections. Direct localization of dmpNA molecules by difference-Fourier synthesis (whether low-resolution data were included or not) was unsuccessful, therefore the simulated annealing option of *FULLPROF* was used, including in the calculation 196 clustered intensities up to $2\theta = 35^\circ$. Owing to steric hindrance, a maximum of two molecules per cell was expected, *i.e.* 0.125 site occupancy for a molecule in a general position. This guest molecule was treated as a rigid body, whose conformation was taken from the crystal structure dmpNA at 293 K (Mak & Trotter, 1965), and with an overall displacement parameter of B_{iso} = 4.0 Å^2. Internal coordinates were defined according to the local frame origin and axes (Fig. 2), and the global position of the molecule was described on the basis of its centre coordinates (X, Y, Z) and the Euler angles θ, φ and χ between the local frame (X_m, Y_m, Z_m) and an orthornormalized cell ($X_0 \parallel a$, $Y_0 \parallel b$, $Z_0 \parallel c$). With this choice, the θ

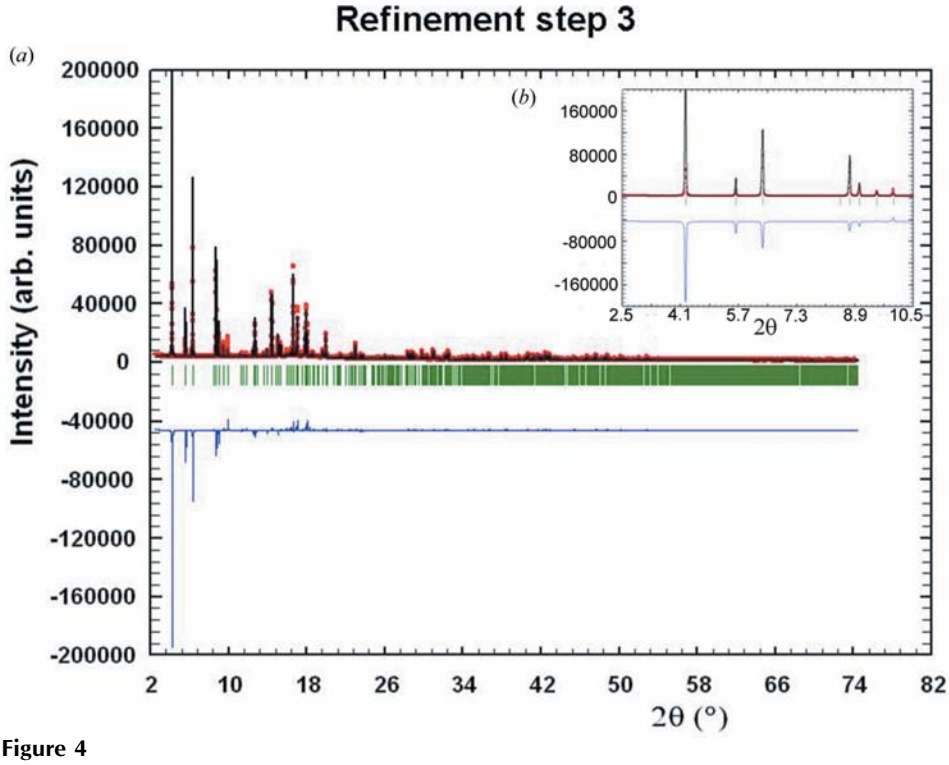

Figure 4
Rietveld fit at the end of the refinement of framework and Na1, Na2 cations of the (dmpNA-MOR) phase at 90 K. (*a*) Full 2θ range; (*b*) zoom on low-resolution Bragg intensities ($2\theta < 10.5^\circ$). Experimental: red points; calculated: continuous black line; difference: continuous blue line. This figure is in colour in the electronic version of this paper.

Table 2
Experimental details.

	90 K	300 K
Crystal data		
Chemical formula	$\|Na_6(O_2NC_6H_4N(CH_3)_2)_{1.94}\|$-$[Al_6Si_{42}O_{96}]$MOR{[001](12-ring)}(*Cmcm*)	$\|Na_6(O_2NC_6H_4N(CH_3)_2)_{1.94}\|$-$[Al_6Si_{42}O_{96}]$MOR{[001](12-ring)}(*Cmcm*)
M_r	202.26	202.26
Cell setting, space group	Orthorhombic, *Cmcm*	Orthorhombic, *Cmcm*
Temperature (K)	90	300
a, b, c (Å)	18.04416 (6), 20.40681 (6), 7.49986 (2)	18.08155 (5), 20.41153 (5), 7.501445 (16)
V (Å^3)	2761.63 (1)	2768.58 (1)
Z	16	16
D_x (Mg m^{-3})	2.000	2.000
Radiation type	Synchrotron	Synchrotron
Specimen form, colour	Parallelepiped, yellow	Parallelepiped, yellow
Specimen size (mm)	2 × 0.2 × 0.2	2 × 0.2 × 0.2
Data collection		
Diffractometer	Spring-8 BL02B2	Spring-8 BL02B2
Data collection method	Specimen mounting: glass capillary; mode: cylinder; scan method: fixed	Specimen mounting: glass capillary; mode: cylinder; scan method: fixed
Absorption correction	None	None
2θ (°)	$2\theta_{min}$ = 0.00, $2\theta_{max}$ = 75.17, increment = 0.01	$2\theta_{min}$ = 0.0653, $2\theta_{max}$ = 75.1653, increment = 0.010001
Refinement		
R factors	R_p = 0.0215, R_{wp} = 0.0316, R_{exp} = 0.006, R_B = 0.0395	R_p = 0.0255, R_{wp} = 0.0368, R_{exp} = 0.0067, R_B = 0.0412
Wavelength of incident radiation (Å)	1.001710	1.001710
Excluded region(s)	0.00–2.50 and 74.50–75.18	0.00–2.50 and 74.50–75.18
Profile function	T–C–H pseudo-Voigt corrected for asymmetry	T–C–H pseudo-Voigt corrected for asymmetry
No. of parameters	116	110
H-atom treatment	Not refined	Not refined
Weighting scheme	w = 1.0/variance(y_{obs})	w = 1.0/variance(y_{obs})
$(\Delta/\sigma)_{max}$	0.05	0.05

Computer programs used: *FULLPROF* (Rodriguez-Carvajal, 1993).

angle between Z_0 (parallel to the cell axis **c**) and the elongation axis Z_m of the molecule is a direct measure of the tilt angle of the molecule inside the large straight channel. Similarly, (X, Y) provides information about the off-centring of the dmpNA from the channel axis. In order to accelerate the simulated annealing calculations, the frozen framework and Na^+ cations were described by partial structure factors. Various starting configurations were tested, from constrained ones where X, Y and θ parameters were restricted (according to a confinement of the molecule in the straight channels) to totally random ones where the molecule was free to sit in the channel walls. All calculations converged to similar solutions, where the molecule lies inside the straight channel, slightly off-centred and tilted. However, because of the comparable scattering power of the symmetrical $NO_2/N(CH_3)_2$ terminal groups of dmpNA, and of the limited resolution, two sets of solutions (4 and 4′) were found by simulated annealing. These sets differ by an exchange of these groups. In both cases the introduction of the molecule in the model led to spectacular amelioration of the agreement factors on subsequent Rietveld refinements, especially for the low-resolution intensities that could not be fitted before (Table 1). Refinement of site occupancy and global displacement parameters of dmpNA was surprisingly stable: the occupancy converged to [0.12114 (5)] close to the maximum expected value (0.125), and the displacement parameter B_{iso} was similar [2.88 (5) Å^2] to that of the Na2 cation. No correlations were detected, even in the final steps where all structural and global parameters were refined together. As expected, the agreement factors for the two dmpNA orientations were close, slightly in favour of hypothesis 4; this ambiguity is addressed further. Except for small discrepancies at low $\sin\theta/\lambda$ caused by asymmetric line profiles, the Rietveld fit was satisfying, even for low-resolution Bragg intensities (Figs. 5*a* and b, hypothesis 4). The corresponding final structural parameters are in the CIF which has been deposited.[1] From the Rietveld refinement, the loading with dmpNA is almost complete with two molecules filling the zeolite channels (IUPAC $|Na_{5.2}(O_2NC_6H_4N(CH_3)_2)_{1.94}|[Si_{48}O_{96}]$·MOR {[001](12-ring)} (*Cmcm*)).

Second harmonic generation requires that, locally, the space group of the commensurate phase is non-centrosymmetric, and has no mirror normal to the dipole axis of the molecules. In the case of MOR, the channels hosting the molecules run along [001], and the subgroup of *Cmcm* of lower index obeying these conditions is $Cmc2_1$. Such a pseudosymmetry was invoked previously for the framework of MOR itself (Alberti *et al.*, 1986; Simoncic & Armbruster, 2004), hence this hypothesis was also tested for structural refinements. Starting from the description of the framework in *Cmcm* previously described, a similar procedure (localization of cations on Fourier maps, of dmpNA molecules with simulated annealing algorithm) was applied. Results are similar from a statistical point of view for both orientations of the molecules [NO_2 or $N(CH_3)_2$ pointing along the c axis] and lead to similar agreement factors (R = 0.0874 and 0.0892, respectively) which are slightly higher than for hypothesis 4. The refined occupancy factor is 0.2421 (1), twice as large as that refined in *Cmcm*, as expected. One can expect such a result because of the global disorder and the similar scattering power for

[1] Supplementary data for this paper are available from the IUCr electronic archives (Reference: CK5032). Services for accessing these data are described at the back of the journal.

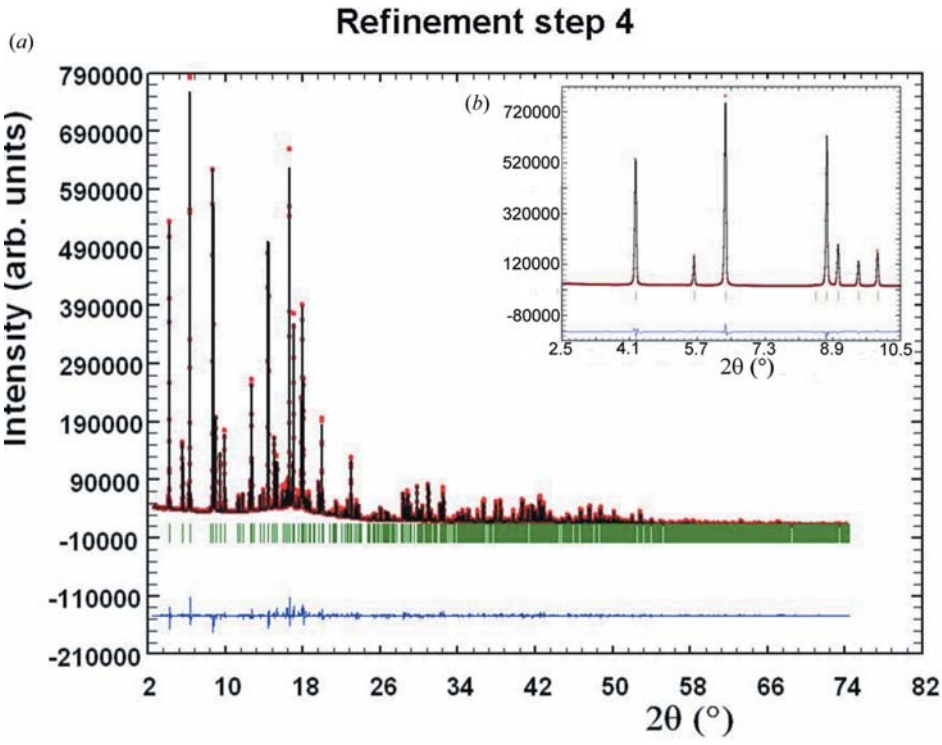

Figure 5
Fit at the end of refinement of (dmpNA-MOR) phase at 90 K. (*a*) Full 2θ range; (*b*) zoom on low-resolution Bragg intensities ($2\theta < 10.5^\circ$). Experimental: red points; calculated: continuous black line; difference: continuous blue line. This figure is in colour in the electronic version of this paper.

X-rays of the symmetric NO_2 and $N(CH_3)_2$ groups of dmpNA.

Moreover, since the framework of MOR exhibits a *Cmcm* (pseudo)symmetry, a perfect, long-range ordering of *p*-*N*,*N*-dimethylnitroaniline molecules along the channels is unlikely. A coexistence of polar $Cmc2_1$ domains of opposite orientation is expected, because of the limited coherence (if any) between neighbouring channels and of the probable disorder inside the channels themselves even though a polar head-to-tail distribution of the molecules is energetically more stable. Hence, the *Cmcm* hypotheses reflect the lack of information on the polar arrangement of the molecules in the channels and the probable coexistence of domains of similar volumes with both orientations of the molecules.

3.2. Modelling of totally disordered dmpNA guest molecules (90 K experiment)

In the model derived from simulated annealing, the dmpNA molecules are disordered over eight sites in the straight channels, where they form tubular clusters (Fig. 6*a*). Such an arrangement may suggest that dmpNA could, in fact, be modelled as a disordered solvent. In order to test this hypothesis, we performed Rietveld refinements, starting from structural model 4 (Table 1) and introducing the 'solvent' contribution as known partial structure factors. The totally disordered dmpNA molecules were modelled by tubes of uniform electron density ρ (Fig. 6*b*) of various internal (r_{int}) and external (r_{ext}) radii, assuming a simple step density profile ($\rho = 0$ if the radius $r < r_{int}$ or $r > r_{ext}$, and $\rho =$ constant elsewhere). The electron density was adjusted to obtain a total of 140 e per unit cell, corresponding to 16 × 0.12114 dmpNA molecules per unit cell. The structure factors were calculated for the full 2θ range by discrete summation on the asymmetric unit ($0 < x < \frac{1}{2}$, $0 < y < \frac{1}{2}$, $0 < z < \frac{1}{4}$), where the electron density was described by 91 × 102 × 19 pixels of ∼ 0.1 Å.

There were 15 configurations, differing by the mean radius $\langle r \rangle$ of the tube and its radial extension Δr, generated, and refinements similar to that performed with the rigid-body description of dmpNA were carried out. For some configurations refinements were not stable and the Na2 displacement parameter became abnormally large.

As expected, these disordered models mainly affect the low-resolution structure factors (see Fig. S1 in the supplementary data). Although these flat density models lead to a large improvement of the agreement factors (supplementary data, Table S1), none of these, whatever the hypothesis, gives a result as good as that obtained with the molecular description of dmpNA (Table 1). For the low-angle part of the pattern ($2.5 < 2\theta < 20^\circ$), which is more sensitive to the inclusion of guest molecules, the R_{Bragg} factor is only reduced to 0.0701, compared with 0.0249/0.0226 for molecule-based models. This supports the hypothesis of a precise localization of dmpNA molecules, as obtained from the previous refinement.

3.3. 300 K experiment

The 300 K diffraction pattern shows the same features as the 90 K experiment. A refinement strategy in four steps similar to that used with 90 K data was applied, and led to similar results. The space group *Cmcm* [a = 18.08155 (5), b = 20.41153 (5), c = 7.50145 (2) Å] is consistent with the pattern, the cation locations are similar, as is the arrangement of the molecules in the [001] channels. The displacement parameters of the dmpNA molecule [B_{iso}(dmpNA) = 4.75 (6) Å^2] are higher than that refined from 90 K data, as expected, but small enough in agreement with a not-totally disordered location of dmpNA. Refinement details are given in Table 1. Full experimental details are given in Table 2.

4. Discussion

4.1. Mordenite framework and cations at 90 K

The topology of the mordenite framework, *i.e.* the connectivity of tetrahedral *T* atoms, is described by the MOR structural type of microporous materials (Baerlocher *et al.*, 2001). This idealized description, independent of chemical composition, is obtained from distance least-squares refinements of a pure SiO_2 framework with mean Si—O distances of 1.61 Å, O—Si—O angles of 109.47° and Si—O—Si angle of 145° corresponding to a relaxed structure (Baerlocher *et al.*, 1977). The MOR structural type has similar cell parameters and the same space group (*Cmcm*) as mordenite, with an asymmetric unit of four *T* atoms and ten O atoms, some of them occupying special symmetry sites (*T*3, *T*4, O4–O10), hence an unusual 180° *T*—O8—*T* valence angle. The MOR framework exhibits a one-dimensional channel system ∥ [001] with 6.5 × 7.0 Å (van der Waals radii included) free apertures limited by 12-membered rings. In addition to these large straight channels, MOR has secondary [010] and [001] small channels limited by elliptical eight-membered rings of 3.4 × 4.8 and 5.7 × 2.6 Å (Fig. 1) which are too small to accommodate guest molecules.

In a real mordenite of mean chemical composition $Na_6Al_6Si_{42}O_{96}\cdot 19H_2O$, approximately 12.5% of *T* sites are occupied by Al atoms. The question of Si,Al ordering on these sites (hence pseudo-centrosymmetry) has been addressed by several authors from experimental (Alberti *et al.*, 1986; Simoncic & Armbruster, 2004; Schlenker *et al.*, 1979) and theoretical (Suzuki *et al.*, 2005) points of view, in relation to the location of acidic sites and extra framework Na^+ cations. In this study a total of 5.2 Na^+ cations (compared with 6.0 predicted from chemical analyses) occupy special positions in [001] small channels. Na1 [$\frac{1}{2}$ 0.0740 (5) $\frac{1}{4}$] and Na2 ($\frac{1}{2}$ 0 0) lie in the 8MR channels (Figs. 7*a* and *b*), whereas the sites in the main 12-membered ring channel (Armbruster & Gunter, 1991, 2001; Schlenker *et al.*, 1979) are empty. Because of their proximity, the global population of these two neighbouring sites should not exceed four cations per unit cell (Maurin *et al.*, 2001; Szostak, 1992). Hence, refinements were performed with constrained site occupancies for Na1/Na2 in order to prevent

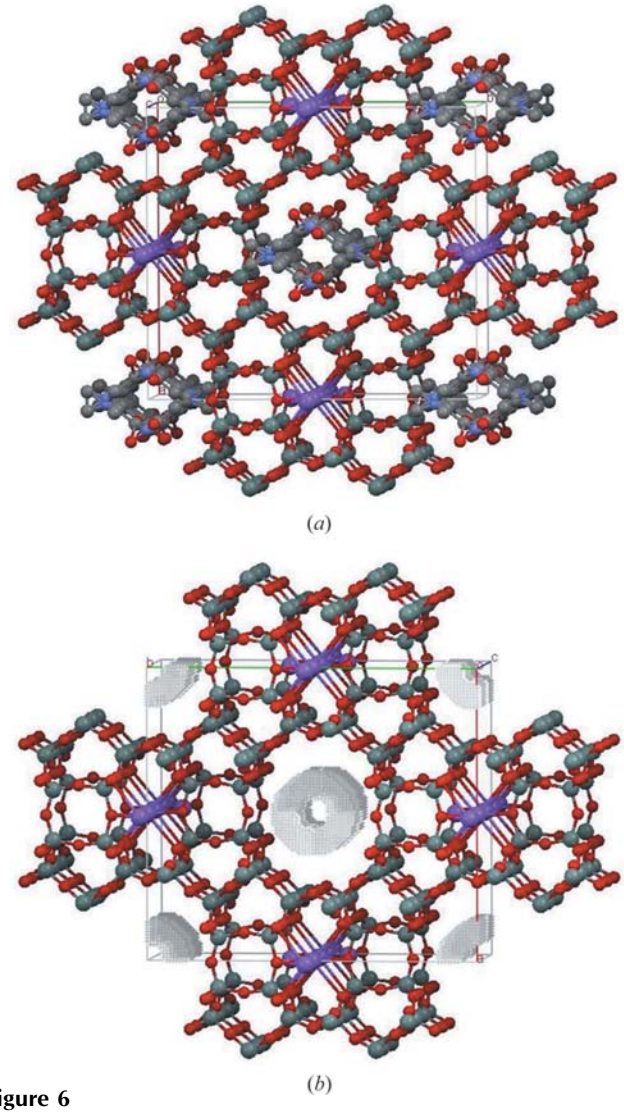

Figure 6
(*a*) Tubular clusters of dmpNA molecules in (dmpNA-MOR) phase at 90 K. For clarity, only C, N and O atoms, which exhibit similar electron density, are shown. (*b*) Tubular electron density model (r_{int} = 1.00 Å, r_{ext} = 2.50 Å, pixel size increased to 0.4 Å on the drawing).

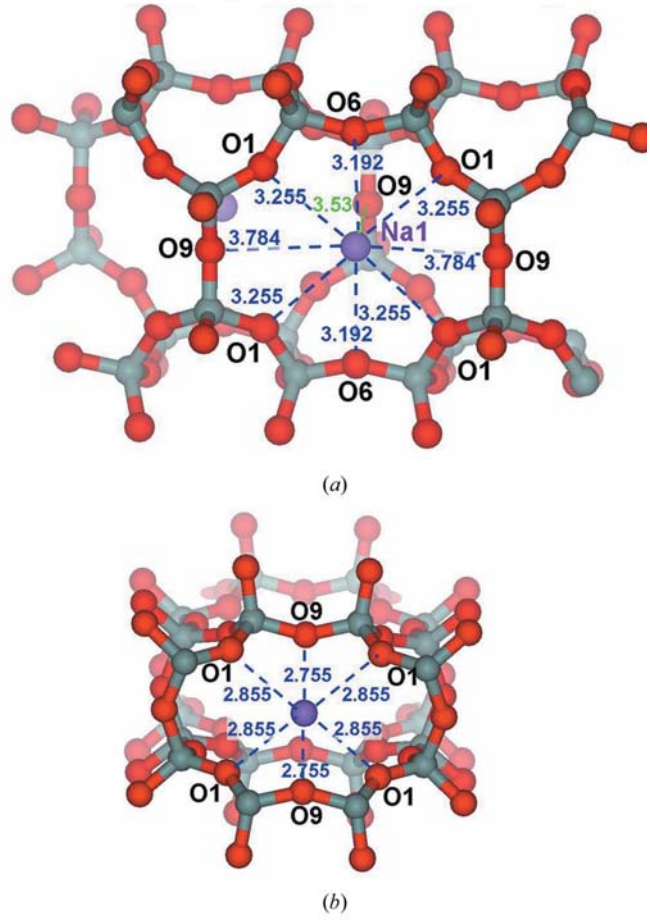

Figure 7
Coordination and environment of (*a*) Na1 cation and (*b*) Na2 cation.

Table 3
Selected distances (Å) and angles (°), with their standard deviations in the framework of the (dmpNA-MOR) phase.

Si1—O1	1.594 (6)	Si2—O2	1.573 (4)	Si3—O1	1.652 (4)	Si4—O2	1.623 (5)
Si1—O3	1.624 (5)	Si2—O3	1.554 (5)	Si3—O1	1.652 (4)	Si4—O2	1.623 (5)
Si1—O6	1.613 (3)	Si2—O5	1.613 (2)	Si3—O4	1.567 (9)	Si4—O4	1.649 (9)
Si1—O7	1.614 (3)	Si2—O8	1.596 (3)	Si3—O9	1.618 (4)	Si4—O10	1.649 (4)
⟨Si1—O⟩	1.61 (1)	⟨Si2—O⟩	1.58 (2)	⟨Si3—O⟩	1.62 (3)	⟨Si4—O⟩	1.64 (1)
O1—Si1—O3	113.7 (5)	O2—Si2—O3	111.0 (4)	O1—Si3—O1	112.1 (4)	O2—Si4—O2	112.3 (4)
O1—Si1—O6	106.9 (4)	O2—Si2—O5	105.5 (3)	O1—Si3—O4	109.8 (6)	O2—Si4—O4	108.3 (6)
O1—Si1—O7	109.5 (5)	O2—Si2—O8	108.3 (3)	O1—Si3—O9	106.3 (4)	O2—Si4—O10	106.6 (3)
O3—Si1—O6	109.3 (4)	O3—Si2—O5	114.1 (4)	O1—Si3—O4	109.8 (4)	O2—Si4—O4	108.3 (6)
O3—Si1—O7	108.0 (3)	O3—Si2—O8	109.5 (3)	O1—Si3—O9	106.3 (4)	O2—Si4—O10	106.6 (3)
O6—Si1—O7	109.5 (3)	O5—Si2—O8	108.3 (3)	O4—Si3—O9	112.6 (7)	O4—Si4—O10	114.7 (7)
⟨O*i*—Si—O*j*⟩	109 (3)					⟨Si*i*—O—Si*j*⟩	153 (11)
Si1—O1—Si3	144.4 (3)	Si3—O4—Si4	162.9 (5)	Si1—O7—Si1	140.2 (3)	Si4—O10—Si4	146.9 (4)
Si2—O2—Si4	146.4 (3)	Si2—O5—Si2	142.8 (2)	Si2—O8—Si2	180.0		
Si1—O3—Si2	160.9 (3)	Si1—O6—Si1	152.2 (3)	Si3—O9—Si3	152.7 (4)		

Table 4
dmpNA-framework contacts with $d(D\cdots A) < 3.40$, $d(\mathrm{H}\cdots A) < 2.33$ Å, $D—\mathrm{H}\cdots A > 100.0°$.

Hydrogen bond (aromatic)	C2—H1···O2	C2—H1···O10	C3—H2···O10
Hypothesis 4			
H···O (Å)	2.052 (4)	2.143 (5)	2.02 (1)
C···O (Å)	2.920 (5)	2.578 (7)	2.49 (1)
Angle (°)	150.4 (4)	106.3 (5)	109.8 (8)

Hydrogen bond (methyl)	C7—H5···O5	C7—H6···O2	C8—H9···O10	C8—H8···O2
H···O (Å)	1.71	1.70	2.33	2.37
C···O (Å)	2.56	2.51	3.19	2.87
Angle (°)	145	137	148	111

Hydrogen bond (aromatic)	C5—H3···O2	C5—H3···O10	C6—H4···O10
Hypothesis 4′			
H···O (Å)	2.187 (4)	2.208 (3)	1.78 (1)
C···O (Å)	2.978 (4)	2.623 (7)	2.43 (9)
Angle (°)	140.5 (4)	105.4 (5)	123.4 (8)

Hydrogen bond (methyl)	C7—H6···O3	C7—H7···O7
H···O (Å)	2.01	2.32
C···O (Å)	2.60	2.69
Angle (°)	116	102

the coexistence of neighbouring Na^+, but the latter led to an unrealistic solution (negative displacement parameters) and were abandoned. Without constraints, the global population (5.2 Na^+/u.c.) exceeds the expected limit of 4. This anomaly may be explained by disorder affecting Na1 and/or partial site occupancy by water molecules despite dehydration. This is supported by the weak coordination of Na1 which is located more than 3 Å away from eight O atoms of a [010] channel aperture [Na1—O6 = 3.192 (7), Na1—O1 = 3.255 (5), Na1—O9 = 3.53 (1), Na1—O9 = 3.784 (2) Å]. The large displacement parameter of Na1 [8.7 (1) $Å^2$] may account for its disorder inside the eight-membered ring; Na1 occupancy should be correlated with B_{iso}, even if not detected during the refinement. In contrast, Na2 almost fully occupies a 4(*b*) Wyckoff position where it is stabilized by six interactions [2 Na2—O9 = 2.755 (7), 4 Na2—O1 = 2.855 (5) Å] which are slightly longer than the sum of their ionic radii [Shannon, 1976; $r(Na^+) = 1.02$, $r(O^{2-}) = 1.35$ Å]; it exhibits a moderate displacement parameter of B_{iso} (Na2) = 3.4 (1) $Å^2$.

Finally, it is noted that the Si—O distances and Si—O—Si valence angles involving the three O atoms O1, O6 and O9 do not depart from those involving other O atoms, in agreement with the weak Na—O 'interactions' (Table 3). The values found are consistent with those obtained from a previous study on a single crystal of Na-mordenite by Armbruster & Gunter (1991) and in other zeolite structures (Porcher *et al.*, 1998, 1999, 2000). Similarly, there is no elongation of Si1—O and Si3—O bonds that may indicate a concentration of Al atoms in these sites, although Na^+ cations are located in the vicinity of Si1 and Si3 sites.

4.2. dmpNA-framework interactions

Fig. 6(*a*) shows the global arrangement of the disordered dmpNA molecules in the [001] 12MR channels as obtained for the best model (hypothesis 4). A more comprehensive view, where only one of the eight symmetry-related molecules per channel is displayed, is given in Fig. 8 for the two possible orientations of dmpNA. The disorder which affects the molecules limits the interpretation of interatomic distances/angles to the description of possible hydrogen bonds between the molecule and framework O atoms O2, O3, O5, O7 and O10 from the channel walls. In addition, one has to keep in mind that the refined models assume a rigid configuration of the dmpNA molecule obtained from its crystal structure (Mak & Trotter, 1965), without any rotation of the methyl groups. For that reason, in Table 4, geometrical data concerning methyl group H atoms (H5–H10) are indicative only. They simply give an insight about possible hydrogen bonds on the basis of donor *D*/acceptor *A* distances and angles: $d(D\cdots A) < R(D) + R(A) + 0.50$ Å, $d(\mathrm{H}\cdots A) < R(\mathrm{H}) + R(A) - 0.12$ Å, $D—\mathrm{H}\cdots A > 100.0°$, with R(H) = 1.10 Å, R(O = acceptor) = 1.35 Å, R(C = donor) = 1.55 Å (Steiner, 1996, 2002; Jeffrey *et al.*, 1985). With this definition, both hypotheses

Table 5
Examples of molecule–framework contacts in zeolite-like or layered materials.

Only contacts with $(D\cdots A) < 3.40$ Å are listed.

$GaPO_4$-ZON (DAB-2)[1]			$AlPO_4$-40[2]			Zincophosphate-THO[3]				$AlPO_4$-SOD[4]		
Diazabicyclo-(2,2,2)-octane			Tetrapropylammonium			Propanediamine				Dimethylformamide		
C—H···O			C—H···O			C—H···O				C—H···O		
3.353	3.235	3.072	3.335			3.292	3.186	3.242		2.900	3.341	
3.292	3.395	3.107										
2.690												
N—H···O	N—H···F	C—H···F				N—H···O						
3.218	2.595	2.975				2.741	3.062	2.921	2.929			
		2.888				3.072	2.918	2.922	2.849			
						2.811	3.029	3.114	3.086			
						3.123	2.916	3.204	2.943			
						2.772	3.317	3.018	2.956			
						2.744	2.926	2.797	2.997			
						2.916	2.857	2.775	2.783			
						2.965	2.915	3.089				
Nu-6 precursor (layered)[5]			SSZ-51[6]			Dipyridinium pyridinium GaPO[7]				Mu-21[8]		
4,4′-Dipyridyl			4-Dimethylaminopyridine			Dipyridinium pyridinium				*N*-Methyl-morpholine		
C—H···O			C—H···O			C—H···O				C—H···O		
2.971	2.874	2.874	3.208	3.310	3.376	3.059	2.833	2.509		3.386	3.369	
2.971												
N—H···O			N—H···O			N—H···O	N—H···F	C—H···F		N—H···O		
2.851	2.601	2.601	2.864			3.011	2.681	2.907		3.115		
2.851										3.103		
Mu-10[9]			ZnPO[10]			Mu-34[11]				Oxalato-MnGallophosphate[12]		
Dimethylammonium			Octakis(dimethylammonium)			Ethylamine				Diethylenetriamine		
C—H···O			C—H···O			C—H···O				C—H···O		
3.031	3.170	3.235	3.320			3.348				2.945		
3.222	3.235		3.368 (OH)			3.331 (apical)						
(N—H···O)			(N—H···O)			(N—H···O)				(N—H···O)		
3.340			2.863	2.829	3.306	2.862	2.719	2.756	2.964	3.008	2.873	3.011
			2.895	2.821		2.915	2.870	3.112	2.887	3.001	2.791	2.906
						2.856	2.966	2.857	3.356	3.051	3.019	
						2.765	2.843	2.831	2.908			
						2.944	2.880	2.817	3.225			
						2.793	2.833	3.090				

References: (1) Meden *et al.* (1997); (2) Ramaswamy *et al.* (1999); (3) Ke *et al.* (2001); (4) Roux *et al.* (2001); (5) Zanardi *et al.* (2004); (6) Morris *et al.* (2004); (7) Weigel *et al.* (1998); (8) Simon-Masseron *et al.* (2003); (9) Soulard *et al.* (1999); (10) Reinert *et al.* (1998); (11) Lakiss *et al.* (2006); (12) Chang & Wang (2005).

4 and 4′ indicate interactions of dmpNA with mordenite *via* three hydrogen bonds involving aromatic H and framework O atoms O2 and O10 with similar mean distances. If the methyl groups are accounted for, supplementary interactions with framework O atoms O3, O5 and O7 are found, especially for hypothesis 4 where the mean distances from methyl (C) to O atoms are smaller. One has to note that hypothesis 4 gives the best agreement factors for the Rietveld fit but, whatever the hypothesis, the global stabilizing interactions appear to be not strong enough to prevent a hopping of the molecule from one site to a symmetry-equivalent site (hence dynamic and static disorder) in the channel. These interactions are however strong enough to preserve the guest–host structure at room temperature.

4.3. Molecule–framework interactions: comparison with the literature and databases

To the best of our knowledge, few (molecule-microporous) structures are described in structural databases or in the literature, most of them dealing with systems where the guest molecule was not localized or is disordered. For example, in the ICSD database (2006) only 27 structures of this type (aluminosilicates and metallophosphates included) are reported, from which only two (Chao *et al.*, 1986; Meden *et al.*, 1997) give a full description of the complex. A more extensive search in the literature gives a few more ordered structures, all (to our knowledge) dealing with complexes (Ramaswamy *et al.*, 1999; Ke *et al.*, 2001; Roux *et al.*, 2001; Zanardi *et al.*, 2004; Morris *et al.*, 2004; Weigel *et al.*, 1998; Simon-Masseron *et al.*, 2003; Reinert *et al.*, 2000; Soulard *et al.*, 1999; Lakiss *et al.*, 2006; Chang & Wang, 2005) where the guest molecule (often an amine) is the template used for the synthesis and is occluded in the framework, and not a molecule introduced after synthesis. Almost all concern (template-metallophosphate) systems, hence structures often include metals in octahedral coordination (in contrast to zeolites) and apical O/OH/F moieties pointing inside the voids and readily interacting with the template. Table 5 summarizes guest molecule–framework interactions in these example structures. Clearly, if the molecule possesses an N—H group, this later forms the stronger (shorter) interactions with framework O/F atoms, either bridging or apical. Then, C—H···O/F bonds have only an auxiliary role, with longer interaction distances. This is the structural imprint of the templating role of the amines during synthesis. If the molecule has only C—H donor groups, as does

dmpNA, but also dimethylformamide (Roux *et al.*, 2001) or tetrapropylammonium (Ramaswamy *et al.*, 1999), these groups ensure the stabilization of the molecule.

In metallophosphates, interactions with apical O/F atoms pointing inside the microporous voids are facilitated by the accessibility of the O/F acceptor which quite often establishes interactions with many molecules with $D\cdots A$ distances ranging between 2.5 and 3.4 Å, and open D—H$\cdots A$ angles (D—H$\cdots A > 130^\circ$). Accordingly, they can be classified as medium to weak, according to Steiner (2002) and Jeffrey (Jeffrey *et al.*, 1985), and dominated by electrostatic/dispersive interactions.

Interaction with bridging O atoms, as in the (dmpNA-MOR) phase are less directional (D—H$\cdots A$ down to 90°) and $D\cdots A$ distance is larger. The acceptor only forms one or two hydrogen bonds with the molecules, as observed in (dmpNA-MOR) crystals (Table 4).

The crystal chemistry of metallophosphates departs significantly from that of zeolites, like mordenite, whose framework is built from fully interconnected AlO_4 or SiO_4 tetrahedra. Because of the paucity of accurate structural information on (molecule-zeolite) systems, a complementary bibliographic search was performed in the Cambridge Structural Database (CSD, Allen, 2002) for structures exhibiting similar local structure, *i.e.* C—H$\cdots$O interactions with bridging T—O—T oxygen atoms. Another more general search was carried out with the search engine *ConQuest*1.7 (Bruno *et al.*, 2002) for C—H$\cdots$O interactions with bridging X—O—X oxygen atoms, where X is any type of atom in tetrahedral coordination. Only intermolecular interactions were looked for, polymeric structures were included in the search, provided that there was no disorder on the fragment.

No restriction on R factor was imposed. The upper limit for $D\cdots$O distances was set to $d = r_D + r_A + 0.2$ Å (r_D, r_A: van der Waals radii of donor and acceptor). H atoms positions were not renormalized and solutions from powder diffraction were accepted. The first search gave seven solutions for N—H$\cdots$O interactions and 29 for C—H$\cdots$O ones, and 1430 and 9326, respectively, if the chemical nature of the tetrahedral atom was not restricted to Si/Al. The scatterplot of O$\cdots$H and C$\cdots$O bond distances, as a function of C—H$\cdots$O angle (Fig. 9), shows that O atoms bonded to two atoms only give rise to weak hydrogen bonds in organic/organometallic compounds, opposite to that observed in the (dmpNA-MOR) complex. Except in the case of polymeric compounds, the stabilization of molecular crystals is achieved through hydrogen bonding and one explanation to this surprising feature could be that in this case, better (more polar/polarizable) acceptors than T—O—T oxygen atoms are available in the structure and that the O$\cdots$H distances are merely contacts. On the contrary, in zeolites, the only acceptors are wall O atoms and, since they are sterically accessible, they ensure the stabilization on the molecule through short hydrogen bonds.

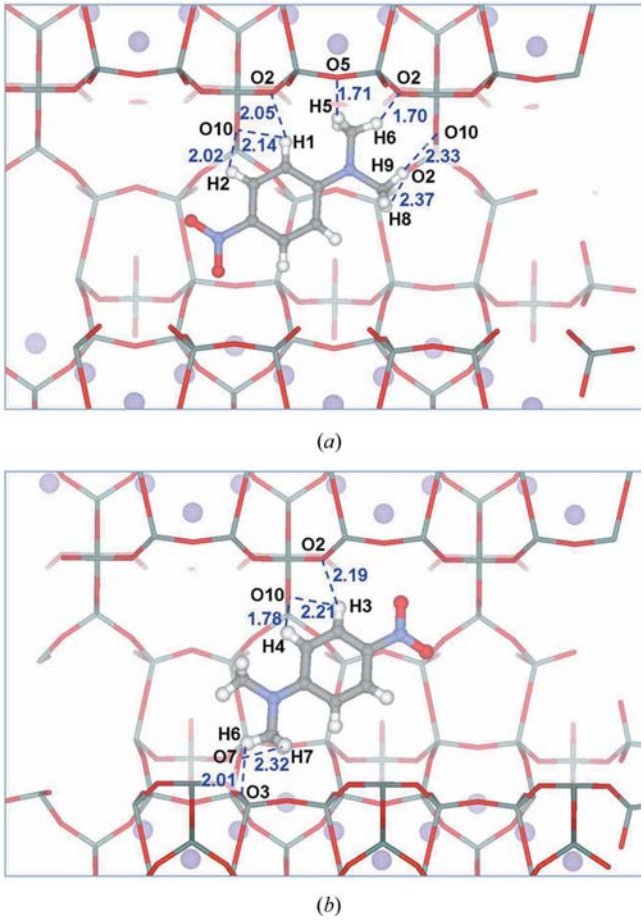

Figure 8
Environment of dmpNA molecules in the channels of mordenite. (*a*) Best model (hypothesis 4). (*b*) Model of hypothesis 4′. For clarity, only one of the eight symmetry-related molecules per channel and bonds with $d(D\cdots A) < 3.40$ Å, d(H$\cdots A) < 2.33$ Å and D—H$\cdots A > 100.0^\circ$ are shown.

4.4. Intermolecular interactions

As a consequence of the dmpNA occupancy factor [0.12114 (5)] the channels of mordenite are crowded by dmpNA molecules close to each other. These polar molecules may equivalently adopt two orientations in the channel (nitro

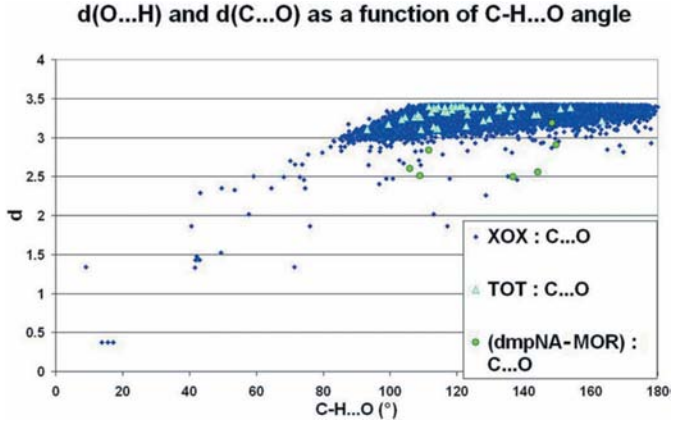

Figure 9
Hydrogen-bond distances C$\cdots$O as a function of C—O$\cdots$H bond angle from CSD search (XOX: oxygen acceptor bonded to two tetrahedral atoms; TOT: oxygen acceptor bonded to two tetrahedral Si or Al atoms) and the present crystal structure.

or dimethylamino moiety toward +**c**) because of the *m*[001] mirror: local intramolecular interactions therefore involve attractive $NO_2\cdots N(CH_3)_2$ or repulsive [$NO_2\cdots NO_2$/$N(CH_3)_2\cdots N(CH_3)_2$] contacts. In the first hypothesis ('head-to-tail' arrangement) these attractive interactions between the donor NO_2 and the acceptor $N(CH_3)_2$ would stabilize the guest arrangement and increase the polarization of dmpNA, with an increased electron density at the aniline nitrogen caused by the electron-donating effect of the alkyl groups and, as a consequence, a bathochromic shift in the optical spectrum. Such a trend is visible on Fig. 3, where the n–π^*/π–π^* transition is shifted by about 50 nm on the reflectance curve compared with pure dmpNA powder ($\sim$ 450 nm). However, this study gives no structural evidence of the existence of dipole chains of dmpNA molecules in the channels, as invoked in other (molecule-zeolite) phases. Most probably $NO_2\cdots N(CH_3)_2$ interactions are favoured, which in turn favour dipole chains. The broadening of the reflectance window, exhibiting unresolved n–π^*/π–π^* transitions, may reflect the variability of the environment and interactions of the disordered molecules in the channels, in relation to the short correlation length of the chains (if any). Finally, the 13.6 Å distance between neighbouring channels probably precludes inter-channel correlations, making an ordered arrangement of dmpNA molecules unlikely on the crystal scale.

5. Conclusions

The new SHG material (dmpNA-MOR) based on the combination of the large pore zeolite mordenite and small hyperpolarizable molecule *p*-*N*,*N*-dimethylnitroaniline shows high loading of guest molecules in the [001] channels with a moderate tilt angle. The molecules are disordered but localized over eight symmetry-related sites, as confirmed by the failure of any attempts to model perfectly disordered guest molecules by uniform cylindrical electron density. Their interactions with the framework O atoms through hydrogen bonds are described on a geometrical basis. Owing to the disorder, the intermolecular interactions could not be properly determined from the structural data, but have been discussed on the basis of UV–vis spectroscopy.

We thank A. Bouché for his technical help in the preparation of the sample. EB is grateful to the French 'Ministère de l'Education Nationale et de la Recherche' for her doctoral fellowship (Allocataire de Recherches). The synchrotron radiation experiments were performed at the BL02B2 in the SPring-8 with the approval of the Japan Synchrotron Radiation Research Institute (JASRI; Proposal No. 2006B1166).

References

Alberti, A., Davoli, P. & Vezzalini, P. G. (1986). *Z. Kristallogr.* **175**, 249–256.
Allen, F. H. (2002). *Acta Cryst.* B**58**, 380–388.
Armbruster, T. & Gunter, M. E. (1991). *Am. Mineral.* **76**, 1872–1883.
Armbruster, T. & Gunter, M. E. (2001). *Rev. Mineral. Geochem.* **45**, 1–67.
Aubert, E., Porcher, F., Souhassou, M. & Lecomte, C. (2003). *Acta Cryst.* B**59**, 687–700.
Aubert, E., Porcher, F., Souhassou, M. & Lecomte, C. (2004). *J. Phys. Chem. Solids*, **65**, 1943–1949.
Aubert, E., Porcher, F., Souhassou, M., Petricek, V. & Lecomte, C. (2002). *J. Phys. Chem. B*, **106**, 1110–1117.
Baerlocher, C., Hepp, A. & Meier, W. M. (1977). *Distance Least Squares Refinement Program DLS-76*. Institut für Kristallographie and Petrographie, ETH, Zurich.
Baerlocher, C., Meier, W. M. & Olson, D. H. (2001). *Atlas of Zeolite Framework Types*, 5th ed. Amsterdam: Elsevier.
Boultif, A. & Louër, D. (1991). *J. Appl. Cryst.* **24**, 987–993.
Bruno, I. J., Cole, J. C., Edgington, P. R., Kessler, M., Macrae, C. F., McCabe, P., Pearson, J. & Taylor, R. (2002). *Acta Cryst.* B**58**, 389–397.
Calzaferri, G., Brühwiler, D., Megelski, S., Pfenniger, M., Pauchard, M., Hennessy, B., Maas, M., Devaux, A. & Graf, U. (2000). *Solid State Sci.* **2**, 421.
Caro, J., Finger, G., Kornatowski, J., Richter-Mendau, J., Werner, L. & Zibrowius, B. (1992). *Adv. Mater.* **4**, 273.
Caro, J., Marlow, F. & Wübbenhorst, M. (1994). *Adv. Mater.* **6**, 413–416.
Chang, W.-M. & Wang, S.-L. (2005). *Chem. Mater.* **17**, 74–80.
Chao, K.-J., Lin, J.-C. & Wang, Y. (1986). *Zeolites*, **6**, 35–38.
Dutta, P. K. (1995). *J. Incl. Phenom. Mol. Recognit. Chem.* **21**, 215–237.
Finger, L. W., Cox, D. E. & Jephcoat, A. P. (1994). *J. Appl. Cryst.* **27**, 892–900.
Fyfe, C. A. & Brouwer, D. H. (2000). *Microporous Mesoporous Mater.* **39**, 291–305.
Ghermani, N. E., Lecomte, C. & Dusausoy, Y. (1996). *Phys. Rev. B*, **53**, 5231–5239.
Hoffmann, K., Marlow, F. & Caro, J. (1996). *Zeolites*, **16**, 281–286.
Hoffmann, K., Marlow, F., Caro, J. & Dähne, S. (1996). *Zeolites*, **16**, 138–141.
ICSD (2006). *Inorganic Crystal Structure Database*, Release 2006/2, http://icsdweb.Fiz-karlsruhe.de.
Jeffrey, G. A., Maluszynska, H. & Mitra, J. (1985). *Int. J. Biol. Macromol.* **7**, 336–348.
Ke, Y., He, G., Li, J., Zhang, Y. & Lu, S. (2001). *New J. Chem.* **25**, 1627–1630.
Komori, Y. & Hayashi, S. (2003*a*). *Chem. Mater.* **15**, 4598–4603.
Komori, Y. & Hayashi, S. (2003*b*). *Langmuir*, **19**, 1987–1989.
Koningsveld, H. van & Koegler, J. H. (1997). *Microporous Mater.* **9**, 71–81.
Kubota, Y., Takata, M., Matsuda, R., Kitaura, R., Kitagawa, S. & Kobayashi, T. C. (2006). *Angew. Chem. Int. Ed.* **45**, 4932–4936.
Kuntzinger, S., Ghermani, N. E., Dusausoy, Y. & Lecomte, C. (1998). *Acta Cryst.* B**54**, 819–833.
Laeri, F., Schüth, F., Simon, U. & Wark, M. (2003). *Host–Guest-Systems Based on Nanoporous Crystals.* Weinheim: Wiley-VCH Verlag GmbH.
Lakiss, L., Simon-Masseron, A., Porcher, F. & Patarin, J. (2006). *Eur. J. Inorg. Chem.* **1**, 237–243.
LeBail, A., Duroy, H. & Fourquet, J. L. (1988). *Mater. Res. Bull.* **23**, 447–452.
Mak, T. C. W. & Trotter, J. (1965). *Acta Cryst.* **18**, 68–74.
Marlow, F., Caro, J., Werner, L., Kornatowsky, J. & Dähne, S. (1993). *J. Phys. Chem.* **97**, 11286.
Marlow, F., Wübbenhorst, M. & Caro, J. (1994). *J. Phys. Chem.* **98**, 12315–12319.
Matsuda, R., Kitaura, R., Kitagawa, S., Kubota, Y., Belosludov, R. V., Kobayashi, T. C., Sakamoto, H., Chiba, T., Takata, M., Kawazoe, Y. & Mita, Y. (2005). *Nature*, **436**, 238–241.
Maurin, G., Senet, P., Devautour, S., Gaveau, P., Henn, F., Van Doren, V. E. & Giuntini, J. C. (2001). *J. Phys. Chem. B*, **105**, 9157–9161.

Meden, A., Grosse-Kunstleve, R. W., Baerlocher, C. & McCusker, L. B. (1997). *Z. Kristallogr.* **212**, 801–807.
Mentzen, B. F. & Lefebvre, F. (1998). *J. Chem. Phys.* **95**, 1052–1067.
Morris, R. E., Burton, A., Bull, L. M. & Zones, S. I. (2004). *Chem. Mater.* **16**, 2844–2851.
Porcher, F., Souhassou, M., Dusausoy, Y. & Lecomte, C. (1998). *C. R. Acad. Sci. II*, **11**, 701–708.
Porcher, F., Souhassou, M., Dusausoy, Y. & Lecomte, C. (1999). *Eur. J. Mineral.* **11**, 333–343.
Porcher, F., Souhassou, M., Graafsma, H., Puig-Molina, A., Dusausoy, Y. & Lecomte, C. (2000). *Acta Cryst.* B**56**, 766–772.
Ramaswamy, V., McCusker, L. B. & Baerlocher, C. (1999). *Microporous Mesoporous Mater.* **31**, 1–8.
Reck, G., Marlow, F., Kornatowski, J., Hill, W. & Caro, J. (1996). *J. Phys. Chem.* **100**, 1698–1704.
Reinert, P., Zabukovec Logar, N., Patarin, J. & Kaucic, V. (1998). *Eur. J. Solid State Inorg. Chem.* **35**, 373–387.
Rodriguez-Carvajal, J. (1993). *Physica B*, **192**, 55–69.
Roux, M. T., Marichal, C., Paillaud, J. L., Fernandez, C., Baerlocher, C. & Chezeau, J.-M. (2001). *J. Phys. Chem. B.*, **105**, 9083–9092.
Sano, T., Wakabayashi, S., Oumi, Y. & Ouzumi, T. (2001). *Microporous Mesoporous Mater.* **46**, 67–74.
Schlenker, J. L., Pluth, J. J. & Smith, J. V. (1979). *Mater. Res. Bull.* **14**, 751–758.
Schulz-Ekloff, G., Wöhrle, D., Van Duffel, B. & Schoonheydt, R. A. (2002). *Microporous Mesoporous Mater.* **51**, 91–138.
Shannon, R. D. (1976). *Acta Cryst.* A**32**, 751–767.
Shantz, D. F. & Lobo, R. F. (1999). *Top. Catal.* **9**, 1.
Simoncic, P. & Armbruster, T. (2004). *Am. Mineral.* **89**, 421–431.
Simon-Masseron, A., Paillaud, J.-L. & Patarin, J. (2003). *Chem. Mater.* **15**, 1000–1005.
Smith, G. S. & Snyder, R. L. (1979). *J. Appl. Cryst.* **12**, 60–65.
Soulard, M., Patarin, J. & Marler, B. (1999). *Solid State Sci.* **1**, 37–53.
Steiner, T. (1996). *Cryst. Rev.* **6**, 1–57.
Steiner, T. (2002). *Angew. Chem. Int. Ed.* **41**, 48–76.
Suzuki, K., Katada, N. & Niwa, M. (2005). *Chem. Lett.* **34**, 398–399.
Szostak, R. (1992). *Handbook of Molecular Sieves*, p. 345. Berlin: Springer.
Takata, M., Nishibori, E., Kato, K., Kubota, Y., Kuroiwa, Y. & Sakata, M. (2002). *Adv. X-ray Anal.* **45**, 377–384.
Thompson, P., Cox, D. E. & Hastings, J. B. (1987). *J. Appl. Cryst.* **20**, 79–83.
Weigel, S. G., Morris, R. E., Stucky, G. D. & Cheetham, A. K. (1998). *J. Mater. Chem.* **8**, 1607–1611.
Wolff, P. M. de (1968). *J. Appl. Cryst.* **1**, 108–113.
Zanardi, S., Alberti, A., Cruciani, G., Corma, A., Fornes, V. & Brunelli, M. (2004). *Angew. Chem. Int. Ed.* **43**, 4933–4937.